

Enhancement of long-range magnetic order by magnetic field in superconducting $\text{La}_2\text{CuO}_{4+y}$

B. Khaykovich,¹ Y. S. Lee,^{2,*} R. W. Erwin,² S.-H. Lee,² S. Wakimoto,³ K. J. Thomas,¹ M. A. Kastner,¹ and R. J. Birgeneau^{3,1}

¹*Department of Physics and Center for Material Science and Engineering, Massachusetts Institute of Technology, Cambridge, MA 02139*

²*Center for Neutron Research, NIST, Gaithersburg, MD 20899-8562*

³*Department of Physics, University of Toronto, Toronto, Ontario M5S 1A7, Canada*

(Dated: October 22, 2018)

We report a detailed study, using neutron scattering, transport and magnetization measurements, of the interplay between superconducting (SC) and spin density wave (SDW) order in $\text{La}_2\text{CuO}_{4+y}$. Both kinds of order set in below the same critical temperature. However, the SDW order grows with applied magnetic field, whereas SC order is suppressed. Most importantly, the field dependence of the SDW Bragg peak intensity has a cusp at zero field, as predicted by a recent theory of competing SDW and SC order. This leads us to conclude that there is a repulsive coupling between the two order parameters. The question of whether the two kinds of order coexist or microscopically phase separate is discussed.

PACS numbers: 74.72.Dn, 75.10.Jm, 75.30.Fv, 75.50.Ee

I. INTRODUCTION

The high-transition-temperature superconductors have dynamic and sometimes static magnetic order,^{1,2,3,4,5,6,7} whereas in conventional superconductors, magnetic and superconducting order involving the same electrons typically do not coexist. It is important to know whether these two kinds of order compete or cooperate with one another, and whether they coexist microscopically or form spatially separate phases. This has been a subject of controversy concerning both experimental results^{1,2,3,4,5,6,7,8,9} and theoretical predictions.^{10,11,12,13,14} In the context of interaction between SC and static SDW order, excess-oxygen-doped $\text{La}_2\text{CuO}_{4+y}$ is especially interesting. The transition temperature to long-range magnetic order (T_m) coincides with the superconducting transition (T_c),⁷ and both transition temperatures $T_c \simeq T_m \simeq 42$ K are the highest achieved in La_2CuO_4 doped by any means, at atmospheric pressure. Since T_c and T_m are so high, it has been suggested that the SC and SDW order enhance one another.⁷ These observations place the oxygen-doped material in strong contrast with La_2CuO_4 doped in different ways, $\text{La}_{2-x-y}\text{Nd}_y\text{Sr}_x\text{CuO}_4$ ⁵ and $\text{La}_{1.88}\text{Sr}_{0.12}\text{CuO}_4$,⁶ in which SC and SDW order appear to compete. This has raised the possibility that the quenched disorder of Sr and Nd ions or the structural distortion resulting from Nd substitution might obscure the observation of the intrinsic interaction between SDW order and superconductivity. By contrast, excess-oxygen-doped $\text{La}_2\text{CuO}_{4+y}$ with $T_c \simeq 42$ K is a stoichiometric compound that exhibits three-dimensional order of the excess oxygen, both parallel and perpendicular to the CuO_2 layers.¹⁵

We report here experimental results on this interesting compound, which shed new light on the interaction

of the SC and SDW orders. We have measured the magnetic field dependence of the SDW Bragg peak and find that the magnetic field enhances the SDW order while resistivity measurements show that, as usual, the field suppresses SC order. We also present detailed transport and magnetization data. We synthesize our neutron scattering results with the results of the muon spin rotation (μSR) experiments on the same samples.^{8,9} These two experimental techniques are complementary; the neutrons probe the long-distance ordering of the Cu spins, while μSR measures the local magnetic field due to the Cu spins at certain positions in the unit cell.

Our paper is organized as follows: In Section II we provide experimental details. Section III is devoted to a presentation of our results. Finally, in Section IV we discuss the results and draw conclusions.

II. EXPERIMENTAL DETAILS

Single crystals of La_2CuO_4 have been grown by the travelling solvent floating zone technique and subsequently oxidized in an electrochemical cell, as described previously.⁷ It requires several weeks of electrochemical oxidation to prepare a fully oxidized crystal with a volume of order 1 cm^3 . SQUID magnetization measurements have been made on a small piece of each sample used for neutron measurements. The magnetization studies evince a sharp single transition to the SC state at $T_c = 42$ K (onset), as well as the absence of weak ferromagnetism, indicating an unobservable amount of remnant undoped La_2CuO_4 . Thermogravimetric analysis has been performed on two small single crystals oxidized to give $T_c = 42$ K. We find oxygen concentrations of $y = 0.10(1)$ and $y = 0.12(1)$. Since our large single crystals have the same T_c we conclude that their chemical composition is $\text{La}_2\text{CuO}_{4.11}$. However one cannot deter-

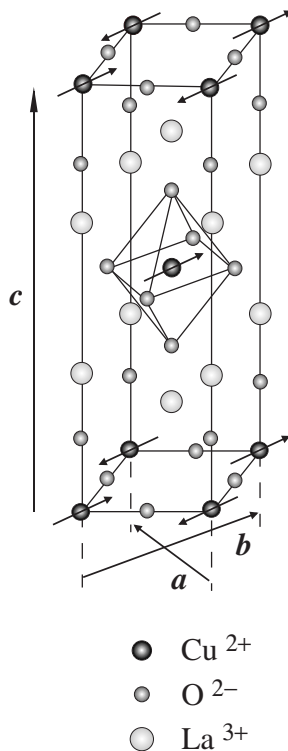


FIG. 1: The unit cell of La_2CuO_4 , depicting the orthorhombic axis and spin directions.

mine the hole density from this oxygen content. Results of Ref. 16 have shown that each intercalated oxygen atom accepts two electrons at very low density but accepts approximately one electron at higher density. Our susceptibility measurements indicate that the hole density is $p \simeq 0.14$, as discussed below.

Neutron measurements have been made on two different samples of $\text{La}_2\text{CuO}_{4.11}$, Sample 1 and Sample 2, each of about 4.5 grams in weight. They originate from different as-grown La_2CuO_4 crystals, but the preparation procedures are identical, and they have the same T_c . Our previous report of SDW order and staging behavior⁷ is based on measurements of Sample 2. Magnetization measurements, as well as NMR and NQR studies by Imai and coworkers¹⁷ have also been made using pieces of Sample 2.

Transport measurements in a magnetic field have been made on pieces of Sample 2, as well as on another small crystal, oxidized to give $T_c = 42$ K. We use the standard 4-probe technique on small rectangular parallelepipeds, approximately $2 \times 1 \times 0.3 \text{ mm}^3$ in size. Thin layers of Ag and, subsequently, Au are evaporated onto the sample surface to form Ohmic contacts. The current used for the four-probe measurements is 0.3 mA, below which the resistivity is found to be current-independent.

Elastic neutron scattering studies were performed at the NIST Center for Neutron Research in Gaithersburg, MD. We used the BT9 and BT2 thermal triple-axis spectrometers with incident neutron energy of 14.7 meV, as

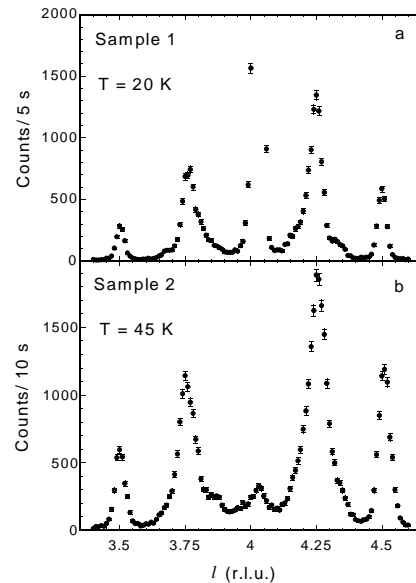


FIG. 2: A scan along the l direction across the staging superlattice positions $(0, 1, l)$ at low temperatures. (a) Sample 1, $T = 20$ K, $E_i = 14.8$ meV, collimation $10^\circ\text{-}40^\circ\text{-}S\text{-}40^\circ\text{-open}$, 3-axis mode (S denotes the sample). (b) Sample 2, $T = 45$ K, $E_i = 35$ meV, collimation $20^\circ\text{-}20^\circ\text{-}S\text{-}20^\circ\text{-open}$, 2-axis mode.

well as the cold-neutron triple-axis spectrometer SPINS with incident energy of 5 meV. A pyrolytic graphite (PG) monochromator and PG analyzer were used, as well as a PG filter to remove higher energy contamination from the incident neutron beam. The magnetic field was applied using a 9 T split-coil superconducting magnet.

III. RESULTS

A. Structural neutron scattering

The structure of La_2CuO_4 is drawn in Figure 1, showing the spin arrangement in the undoped antiferromagnet. Because of a small tilt of the CuO_6 octahedra relative to the c -axis, the crystal structure is actually orthorhombic. We therefore use the orthorhombic unit cell with a and b along the diagonals of the square and c perpendicular to the layers.

Previous studies^{7,18} show that the excess oxygen in $\text{La}_2\text{CuO}_{4+y}$ is not distributed uniformly, but rather has a sine-density-wave modulation that is periodic along the c -axis. The tilt angle of the CuO_6 octahedra changes sign across the planes containing the most oxygen, so the tilt reversal occurs every n th CuO_2 layer. This behavior is called staging, and the sample with tilt reversal every n th layer is called stage- n .^{7,18} The results reported here are for crystals that are stage-4.

Figure 2 shows the intensities of neutron scattering from nuclear Bragg peaks along the $(0,1,l)$ direction. The

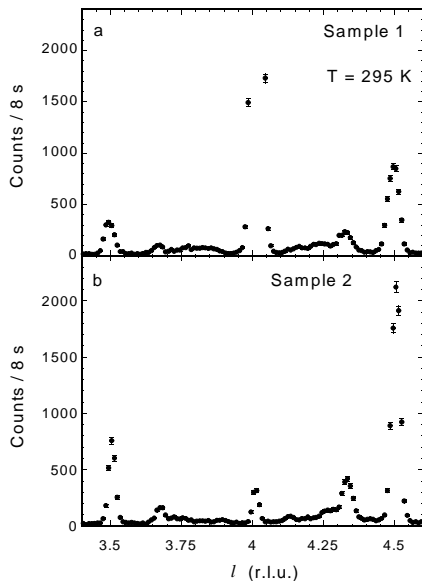


FIG. 3: A scan across the staging positions (0, 1, l) at room temperature, $T = 295$ K. $E_i = 5$ meV, collimation 32'-40'-S-80'-open, 3-axis mode. (a) Sample 1, (b) Sample 2.

undoped crystals have peaks at l even, and a small residue of this can be seen at $l = 4$ in each scan, showing that a small component of the parent $Bmab$ structure remains in each crystal. There is also a very small amount of the stage-6 compound. The two peaks displaced by ± 0.25 reciprocal lattice units (r.l.u.) around $l = 4$ correspond to stage four. Since the unit cell spans two CuO_2 layers, the position $1/4$ corresponds to a period of eight layers. However, as discussed previously,¹⁸ the superlattice peak at $1/4$ comes from the ordering of the tilt angle of the CuO_6 octahedra, which has an antiphase domain boundary every fourth layer, giving an overall periodicity of eight layers. Presumably, the antiphase domain boundary allows more room for intercalated oxygen whose density modulation has a period of four layers.

The peak displaced by 0.5 r.l.u. might appear, at first sight, to result from a stage-2 component. However, it most likely results, instead, from the scattering from both the intercalated oxygen itself and the concomitant displacements of the atoms around the intercalants. Recent studies¹⁵ have shown that in these samples the oxygen is three dimensionally ordered with a period along the c axis of four layers, corresponding to a wavevector displaced by 0.5 r.l.u. The three-dimensional ordering of the intercalated oxygen persists up to 330 K, whereas the stage-4 octahedral tilt ordering is lost above 295 K. Figure 3 shows that the peaks displaced by $1/4$ r.l.u. are missing at room temperature, whereas those displaced by $1/2$ remain. When the crystal is *quenched* from above 330 K, the three-dimensional ordering of the oxygen intercalants is lost and the peak at $1/2$ is not seen at low T , even though the octahedral tilt ordering, evinced by the

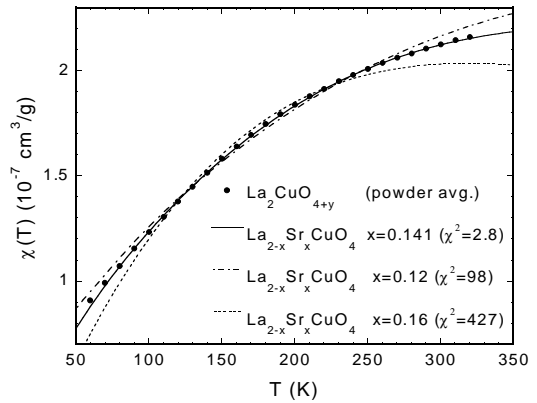


FIG. 4: Temperature dependence of χ in $\text{La}_2\text{CuO}_{4+y}$ (Sample 2) compared with $\text{La}_{2-x}\text{Sr}_x\text{CuO}_4$. One set of measurements was taken with the field alignment $H \parallel c$ and another set was taken with $H \parallel ab$. The powder-averaged susceptibility $\chi(T)$ was calculated from our data via $\chi(T) = \frac{1}{3}\chi^c + \frac{2}{3}\chi^{ab}$. The curves correspond to the scaling function F with parameters obtained from $\text{La}_{2-x}\text{Sr}_x\text{CuO}_4$ for different doping levels x . We extract the functional form of F from Ref. 26, a study of polycrystalline $\text{La}_{2-x}\text{Sr}_x\text{CuO}_4$. The “ χ^2 ” goodness-of-fit (not to be confused with susceptibility) is displayed next to each fit.

peak at $1/4$, is present.¹⁵ We conclude that the crystals are stage-4 with very small inclusions of the oxygen-poor $Bmab$ phase as well as a small amount of stage 6. That the peaks at $1/4$ and $1/2$ come from a single phase is confirmed by observation that the relative intensities of the these two peaks in Fig. 2 are almost the same for the two samples.

B. Magnetization

We next discuss measurements of the uniform magnetic susceptibility $\chi(T)$ in our excess oxygen-doped samples and their relationship to similar measurements in the Sr-doped material $\text{La}_{2-x}\text{Sr}_x\text{CuO}_4$, which allow us to estimate the hole concentration. The normal state susceptibility of $\text{La}_{2-x}\text{Sr}_x\text{CuO}_4$ depends on the temperature T and hole concentration p according to $\chi(p, T) = \chi_0(p) + \chi^{2D}(p, T)$, where χ_0 is a temperature-independent constant. As shown in Refs. 25 and 26, the temperature-dependent term $\chi(T)$ follows a scaling form $\chi^{2D}(p, T/T_{max})/\chi^{2D}(p) = F(T/T_{max}(p))$, where F is the scaling function. This scaling is found to describe the data for $\text{La}_{2-x}\text{Sr}_x\text{CuO}_4$ for a wide range of p , up to $p = 0.26$.^{25,26} The powder-averaged susceptibility of our $\text{La}_2\text{CuO}_{4.11}$ is shown in Fig. 4. The three lines are fits using the scaling function F with the parameters χ_{max}^{2D} and T_{max} chosen to match those in $\text{La}_{2-x}\text{Sr}_x\text{CuO}_4$ with $x = 0.141, 0.12$, and 0.16 , respectively. We find that the curve corresponding to $p = 0.141$ best describes the data, suggesting that the hole concentration for stage-4

$\text{La}_2\text{CuO}_{4.11}$ is $p \simeq 0.14$. The fact that this functional form fits both $\text{La}_{2-x}\text{Sr}_x\text{CuO}_4$ and $\text{La}_2\text{CuO}_{4.11}$ suggests that the hole homogeneity is similar for the two materials, at least for temperatures above T_c . Thus the hole concentration appears to be quite uniform even though the oxygen concentration varies periodically along the c axis.

The undoped component of these crystals is fractionally very small, as we conclude from the following observations: The weakly doped antiferromagnet reveals itself as a peak in the magnetic susceptibility at about 260 K, which arises from hidden weak ferromagnetism. At fields high enough to induce the weak ferromagnetic transition, the moment induced can be used to measure the volume of antiferromagnet in the sample.¹⁹ SQUID magnetization measurements at high fields show that this signature of antiferromagnetic order becomes unobservable as a result of electro-chemical doping, implying that the antiferromagnetic inclusions in our crystals correspond to at most a few per cent of their volume. Similarly, we can use the intensity of inelastic scattering near the antiferromagnetic Bragg peak, resulting from spin waves, to measure the undoped fraction.⁷ No commensurate component is detectable in inelastic scans, confirming that the antiferromagnetic fraction is very small. These observations are equally true for both Sample 1 and Sample 2.

C. Elastic magnetic scattering

As reported previously, the staged compound exhibits two dimensional static SDW order with a periodicity in the square CuO_2 layers that is approximately 8 times that of the underlying lattice, consistent with the stripe model of Tranquada *et al.*⁵ This manifests itself in elastic neutron scattering as four peaks around the 2D antiferromagnetic zone centers $(1,0,l)$ and $(0,1,l)$. (Recall that we are using an orthorhombic unit cell.) Thus, the first quartet of SDW Bragg peaks is at $Q = (1 \pm \delta_h, \pm \delta_k, 0)$. (See the insets of Fig. 5). For Sr doped La_2CuO_4 , the incommensurability (δ_h, δ_k) depends on doping, but for the stage-4 compound we always find the values $\delta_h = 0.114$ and $\delta_k = 0.128$ r.l.u., corresponding to a shift of 0.121(2) r.l.u. for the tetragonal unit cell, close to the value for Sr concentration 1/8 per Cu atom.⁶

Figures 5(a,b) show the SDW peaks at $(0.89, 0.128, 0)$ for Sample 1; similar data are presented in Fig. 5(c,d) for Sample 2 with the identical spectrometer configuration, so a direct comparison between the two samples can be made. Scans along two perpendicular directions in reciprocal space, h and k , are shown for each sample. Comparing the two samples we see that the peak positions are identical, and the widths are similar, but the intensity of the signal for sample 2 is about twice as large as that for sample 1.

The full width at half maximum of the peak, 0.008 r.l.u., is resolution limited for this spectrometer config-

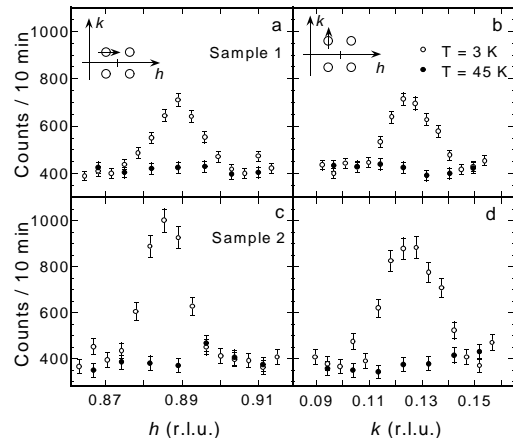


FIG. 5: Neutron elastic scattering from a SDW Bragg peak at zero applied field. The sample was oriented such that the neutron wave vector transfer Q was parallel to the ab , Cu-oxygen, planes. The reciprocal lattice position is $Q = (0.89, 0.128, 0)$. (a) and (b) are scans for Sample 1 along reciprocal space directions h and k , respectively. (c) and (d) are scans for Sample 2 along h and k , respectively. The insets show schematically the reciprocal space and the scan directions. The temperatures are 3 K (open circles) and 45 K (dots) and the collimation is 32'-40'-20'-open, $E_i = 5$ meV.

uration, which indicates that the SDW order has a correlation length greater than 600 Å. Previous studies of the stage-4 crystal have indicated that the SDW is ordered over distances ≥ 600 Å within the CuO_2 plane and there is short-range order (~ 13 Å) perpendicular to the planes. The three-dimensional structure is consistent with a collinear SDW, with the *local* spin structure identical to that of the undoped insulator.⁷

Our most surprising results involve the magnetic field dependence of the SDW Bragg peak. Figure 6 shows typical scans across one of the incommensurate peaks for Sample 1 with and without a magnetic field applied parallel to the c axis. When the sample is cooled in an applied field of 7.5 T, the scattering intensity grows dramatically. Scans along both h and k demonstrate that the peak position and width remain the same within the errors when the field is applied. The same relative increase in intensity is observed at incommensurate positions near different reciprocal lattice points, using different neutron energies (5 and 14.7 meV) and on different spectrometers. Sample 2 shows similar results, albeit with a smaller in-

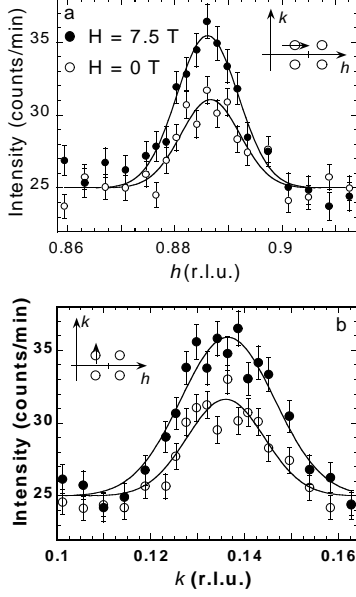


FIG. 6: SDW peaks with and without an applied field at the same spectrometer configuration as for Fig. 5. The open circles are for zero field and the filled circles are for $H = 7.5$ T. The lines are the results of Gaussian fits. The inset shows schematically the position and scan direction in reciprocal space. The field is applied parallel to the c -axis, perpendicular to the planes. The Bragg peak shown occurs at $\mathbf{Q} = (0.886, 0.132, 0)$ and the temperature is $T = 1.5$ K. The collimation is $32'-40'-20'$ -open, $E_i = 5$ meV. These results are for Sample 1 with scans along (a) h and (b) k .

crease in the peak intensity, as discussed further below. Because the sample is mounted in the split-coil magnet to allow application of the field in the c direction, we are able to measure scattering only in the ab plane and can not scan the momentum along c .

The fact that the increased scattering at high fields is at exactly the same position in reciprocal space as that at zero field puts strong constraints on any possible theoretical models. This is especially striking because the peak occurs at a position that is incommensurate in both the a and b directions. Specifically, the increase must reflect an enhancement or a proliferation of the existing SDW order rather than the creation of a new SDW state, for example, in the vortex cores.

D. Onset of SDW and SC order

Figure 7 shows the SDW peak intensity (a) and the resistivity (c) at different applied fields as functions of temperature. It is clear that the applied magnetic field

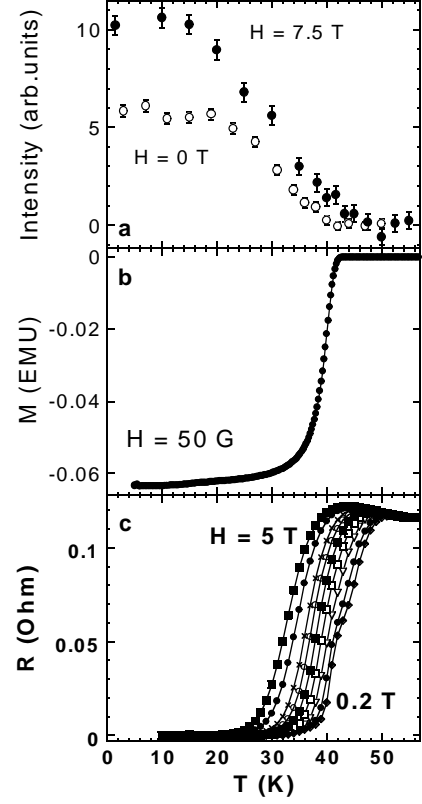


FIG. 7: Temperature dependence of the Bragg peak intensity, superconducting shielding and in-plane resistivity. (a) The peak intensity for Sample 1 at zero field (open circles) and at 7.5 T (filled circles). The peak position, collimation and energy are the same as for Fig. 5. The points are calculated by averaging longitudinal and transverse scans around the peak position; a constant background has been measured and subtracted. (b) The magnetization at small field showing the sharp onset of superconductivity at the same temperature at which the SDW order sets in. (c) The in-plane resistance vs. temperature at applied fields of 0.2, 0.5, 1, 1.5, 2, 2.5, 3, 4, and 5 T. The crystal was oriented by a Laue diffractometer in order to ensure that the transport current was parallel to the ab -planes, while the magnetic field was applied parallel to the c -axis, as in the neutron scattering experiments.

results in an increase of the amplitude of the magnetic Bragg peak over the entire range of temperatures, whereas there is, at most, a very small increase in the SDW ordering temperature. On the other hand, the SC transition temperature, as determined by the onset T_R of the decrease in resistivity, shifts substantially toward lower temperature with increasing field. Similar behavior of the resistivity in a magnetic field has been reported for Sr-doped $\text{La}_{2-x}\text{Sr}_x\text{CuO}_4$ at similar doping levels.²⁰ Clearly, $T_R \simeq 50$ K in zero field, is considerably higher than $T_c \simeq 42$ K measured by the onset of diamagnetism (Fig. 7b). This is possibly the result of SC filaments

that form at higher T and shunt the transport current but do not give rise to a large diamagnetic signal. The SDW onset at $T_m \simeq 42$ K coincides with the magnetically determined T_c .

These results show that the coincidence between T_c and T_m occurs only for $H = 0$, which thus becomes a special point in the phase diagram. A similar coincidence between T_c and T_m at zero field has recently been observed in more lightly doped $\text{La}_2\text{CuO}_{4+y}$ (stage 6) with $T_c = 34$ K.¹⁵

The transport measurements in Fig. 7 have been made with the current and voltage contacts placed on the top surface of a crystal. This makes it difficult to determine even nominal resistivity, given the high electrical anisotropy of $\text{La}_2\text{CuO}_{4+y}$. Measurements on a different sample, with contacts positioned on the side surfaces, have resulted in $\rho_{ab}(0) \simeq 2$ m Ω -cm, which is an order of magnitude higher than that of the best optimally-doped samples of $\text{La}_{2-x}\text{Sr}_x\text{CuO}_4$. The high value of resistivity is similar to that reported in Ref. 20 for $\text{La}_{1.88}\text{Sr}_{0.12}\text{CuO}_4$ (1/8 Sr-doping), which shows a static SDW similar to that in our samples. This suggests that the large resistivity may be related to the incipient SDW order. However, our samples often contain a number of small cracks that appear to grow during the electro-chemical doping. This makes it impossible to accurately determine the current density, so conclusions from the high resistivity must be drawn with caution.

E. Field dependence of the elastic magnetic scattering

In order to elucidate the origin of the increase of the SDW peak amplitude, we have carried out measurements of the intensity of the elastic neutron scattering as a function of field. The results for both samples are presented in Figure 8. Surprisingly, we find that the increase of the intensity with field up to $H = 9$ T is approximately proportional to $|H|$ rather than H^2 . This makes $H = 0$ a singular point; that is, $I(H)$ is not analytic at $H = 0$. We have confirmed that the scattering intensity depends only on the magnitude and not on the sign of the field.

As is clear from Fig. 8, the relative increase of the SDW peak intensity is about twice as large for Sample 1 as it is for Sample 2. Since the SDW peak intensity at zero field is about twice as large for Sample 2 as for sample 1, the absolute intensity change is similar for the two crystals. The SDW intensity has been normalized to the mass of the crystal for each sample. We have checked that the intensities of the nuclear Bragg peaks are consistent with this normalization.

Enhancement of SDW long-range order by a magnetic field has also been observed in Sr-doped $\text{La}_{2-x}\text{Sr}_x\text{CuO}_4$, $x \approx 1/8$.²⁰ The authors of Ref. 20 have not determined the field dependence of the peak intensity. Related effects have been observed in optimally and slightly under-doped $\text{La}_{2-x}\text{Sr}_x\text{CuO}_4$.^{21,22}

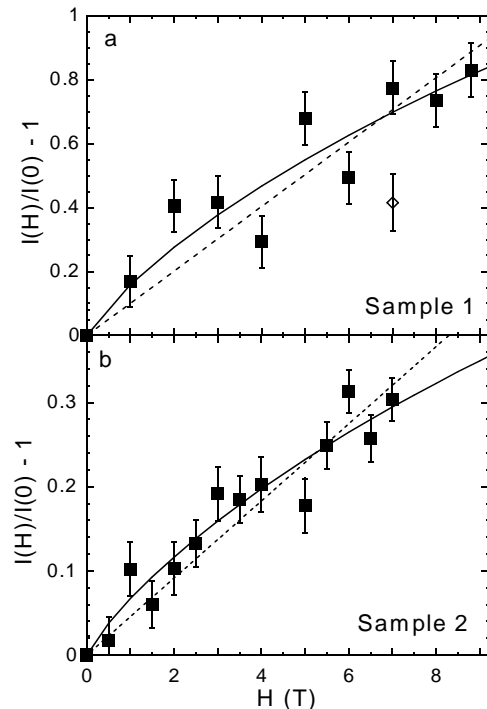


FIG. 8: Relative change in SDW peak intensity above background vs. field for (a) Sample 1 and (b) Sample 2. The filled squares are for measurements made after cooling in a field (FC). The initial neutron energy is $E_i = 14.7$ meV (BT-2 spectrometer). The background at 50 K (found to be independent of field) has been subtracted and the difference is then normalized to the zero-field value. The dashed line assumes $\Delta I \sim |H|$, whereas the solid line corresponds to the function given in ref. 28, $\Delta I \sim H/H_{c2} \ln(3H_{c2}/H)$. For the latter we have fixed H_{c2} at 60 T, so that the only free parameter is the prefactor. We have also performed a zero-field cooled (ZFC) measurement (diamond in the figure), in which a field of 7 T is applied after the sample is first cooled to 1.5 K.

As expected, the zero-field-cooled (ZFC) intensity (the point at 7 T for Sample 1) is reduced significantly, compared to the field-cooled (FC) value, but it is still higher than the zero-field value. The magnetization of $\text{La}_2\text{CuO}_{4+y}$ is irreversible at 1.5 K and 7 T because of the pinning of vortices. When the superconductor is cooled in a field, pinned magnetic flux lines permeate the bulk of the sample, and the magnetic field is expected to be distributed homogeneously. This is because the London penetration length $\lambda \simeq 2200$ Å is much larger than the inter-vortex distance of 150 Å at 7 T. However, when the field is applied after the superconductor is cooled to 1.5 K, the magnetic field penetrates only partially into the bulk of the sample since strong pinning prevents vortices from moving freely. Therefore, the bulk of the sample is better shielded from the magnetic field after ZFC and the SDW peak amplitude is therefore smaller than after FC.

IV. DISCUSSION AND CONCLUSIONS

Since we observe both SC and SDW order it is natural to ask whether these occur in a single phase or in separated phases. In particular, we must consider the possibility that phase separation results from inhomogeneity in the hole concentration. As discussed above, the magnetic susceptibility suggests a uniform hole density. Additional information about variations in the hole concentration comes from a detailed NMR and NQR study carried out by Imai and coworkers on one of our $\text{La}_2\text{CuO}_{4.11}$ samples.¹⁷ Interestingly, the $^{63,65}\text{Cu}$ NQR line profiles and positions turn out to be nearly identical in $\text{La}_2\text{CuO}_{4.11}$ and $\text{La}_{1.865}\text{Sr}_{0.135}\text{CuO}_4$. This indicates, first, that the two materials have comparable hole concentrations and second, that the distribution of electric field gradients at the Cu sites in the two materials is the same implying that they have comparable homogeneities. This also necessitates that in $\text{La}_2\text{CuO}_{4.11}$ there is no measurable difference in hole concentrations for the different CuO_2 layers.

One of the best measures for the homogeneity of La_2CuO_4 -based systems is the sharpness of the tetragonal-to-orthorhombic phase transition. From previous studies of this transition we know that crystals of $\text{La}_{2-x}\text{Sr}_x\text{CuO}_4$, grown by the travelling solvent floating zone technique, have quite uniform Sr distributions. Technically, the sharpness of the structural phase transitions implies that any correlations of the local phase transition temperatures at distance r , due to a tendency of the Sr dopants to cluster, must fall off faster than r^3 .²⁷ Of course, there is local disorder caused by the Sr^{2+} dopants, but this is absolutely statistical so that on large length scales the material is homogeneous. The fact that $\text{La}_2\text{CuO}_{4.11}$ has an identical $^{63,65}\text{Cu}$ NQR line profile to that in $\text{La}_{1.865}\text{Sr}_{0.135}\text{CuO}_4$ requires that it be similarly homogeneous.

Inelastic neutron scattering results also give strong evidence for the homogeneity of the doping in our crystals. The width of the incommensurate inelastic peaks, reported in Ref. 7, is as small as that of the narrowest peaks observed in $\text{La}_{2-x}\text{Sr}_x\text{CuO}_4$. Since the incommensurability varies continuously with the doping in $\text{La}_{2-x}\text{Sr}_x\text{CuO}_4$,³ an inhomogeneous hole concentration should result in an increase in the width of the inelastic peaks. Furthermore, the width at $x = 0.125$ is significantly smaller than that at other x 's, so our narrow inelastic peak indicates that the hole concentration is quite uniform.

Our field-enhanced magnetic scattering has interesting implications. The singular dependence of the SDW amplitude on applied field excludes a purely magnetic mechanism for the phenomenon such as a suppression of fluctuations of the ordered moment by the applied field, as suggested by Katano *et al.*²⁰, or an increase in the correlations along the c -axis. The intensity of a magnetic Bragg peak $I(H)$ is proportional to the square of the ordered staggered moment, $I(H) \sim |M^\dagger|^2$. By symmetry,

the first non-zero correction to M^\dagger must be of second order in field: $\Delta M^\dagger(H) \sim H^2$. Therefore, the leading correction to the intensity from a purely magnetic mechanism must be quadratic in the field $\Delta I(H) \sim H^2$, rather than $\Delta I(H) \sim |H|$, as found experimentally.

The linear increase of the magnetic signal with $|H|$ suggests that the effect originates from magnetic flux lines penetrating the sample in the superconducting state. Indeed, since every vortex carries one magnetic flux quantum, the number of vortices is proportional to $|H|$. The role of vortices has been emphasized in Reference 20 and in a closely related experiment on inelastic and elastic neutron scattering from optimally doped $\text{La}_{2-x}\text{Sr}_x\text{CuO}_4$ ($x=0.163$) in a magnetic field.²¹ The latter experiment has revealed an increase with field of the intensity of low (but non-zero) energy spin excitations at the incommensurate positions. The low-energy fluctuations exist in the normal state, but they are suppressed below T_c in zero field because of the opening of a gap for spin excitations. The authors of reference 21 ascribe the increase of the subgap fluctuations below T_c with applied field to fluctuations toward magnetic order in the vortex cores. A very recent paper by B. Lake *et al.*²² discusses neutron measurements on $\text{La}_{1.9}\text{Sr}_{0.1}\text{CuO}_4$. Lake *et al.* observe results that are consistent with ours, despite the fact that the SDW order is known to be of shorter range in $\text{La}_{1.9}\text{Sr}_{0.1}\text{CuO}_4$ than in $\text{La}_2\text{CuO}_{4.11}$.³

A recent theoretical model^{28,29} for homogeneous coexistence of SDW and SC order explains the singular $\sim |H|$ dependence of the intensity in a natural way. In this model the SDW order parameter $|\phi|^2$ is directly coupled via a positive (repulsive²⁹) coupling coefficient to the superconducting order parameter $|\psi|^2$. The singular increase of the peak intensity results from the singular response of a superconductor to an applied magnetic field. In the presence of vortices, the SC order parameter is reduced in the entire volume of the superconductor, even outside the vortex cores,³⁰ thus causing an increase in the magnetic order parameter because of the positive coupling between $|\phi|^2$ and $|\psi|^2$. Since the SDW correlation length spans many inter-vortex distances, $|\psi|^2$ is averaged over the regions outside the cores. As a result, $|\phi|^2$ is proportional to the absolute value of magnetic field, with a logarithmic correction. This, in turn, leads to the approximately linear increase of the SDW peak intensity at small fields and non-zero derivative dI/dH at $H = 0$. We show in Fig. 8 the form $\Delta I \sim H/H_{c2} \ln(3H_{c2}/H)$ predicted by ref. 28, which describes our data quite well. The fit has only one adjustable parameter since H_{c2} is fixed at 60 T.³¹

Measurements of muon spin relaxation (μSR) have been made on our Sample 2.^{8,9} At temperatures well below T_c the muons' spins precess in an internal magnetic field distribution, which appears to be very similar to that resulting from the SDW in $\text{La}_{1.47}\text{Nd}_{0.4}\text{Sr}_{0.13}\text{CuO}_4$. However, the signal from Sample 2 corresponds to only a fraction, $\sim 40\%$, of the muons experiencing the field.^{8,9} This suggests that the system has spatially separated

into magnetically (SDW) ordered and non-magnetic phases. The average precession frequency reaches its low-temperature value quite abruptly below the SC T_c in $\text{La}_2\text{CuO}_{4.11}$, whereas it increases gradually below the SDW transition in $\text{La}_{1.47}\text{Nd}_{0.4}\text{Sr}_{0.13}\text{CuO}_4$. This suggests that putative microscopic phase separation occurs at T_c .³² Modelling of the μSR signal^{8,9} suggests that the typical size of the magnetic regions is of order 15-50 Å. Note that μSR measurements are strongly suggestive but not conclusive about the volume fraction and size of the superconducting regions.

This model⁹ of microscopic phase separation may help explain the difference in the field dependence between Sample 1 and Sample 2 (see Fig. 8). We assume that the flux penetrates non-magnetic and SDW regions at random, but the field enhances SDW order primarily in the non-magnetic phase. The field-induced change in F , the fraction of the sample primarily in the SDW phase, is proportional to the fraction $1 - F$ primarily in the non-magnetic phase. Therefore, the relative change of the Bragg peak with field, at small field, is expected to be proportional to $(1 - F)/F$. The muon measurements tell us that for Sample 2, $F_2 \sim 0.4$. Since the Bragg peak intensity for Sample 2 is twice that of Sample 1, we would expect $F_1 \sim 0.2$ and the relative change with field would be about 2.5 times smaller for Sample 2 than for Sample 1, in agreement with observation. Essential to this argument is the experimental fact that the detailed geometry of the SDW scattering at high fields is identical to that at zero field.

Since the non-magnetic (or weakly magnetic) regions are superconducting, we propose that the enhancement of SDW order is the result of the Demler *et al.*²⁸ mechanism discussed above. Of course, the magnetic regions may also be superconducting, but since the SDW order parameter in them must be large, flux penetration cannot enhance it significantly.

If, as suggested by μSR , 40% or less of each layer of Sample 2 consists of SDW ordered regions that are only 15-50 Å in size, it is at first surprising that long range SDW order is observed, even in zero field. One might have ascribed this to simple nearest-neighbor percolation, since 40% is close to the percolation threshold in two dimensions. However, Sample 1 has only half the SDW concentration, judging from the size of the Bragg peak, and it also shows long-range order. Furthermore, muon experiments on a crystal of $\text{La}_{1.88}\text{Sr}_{0.12}\text{CuO}_4$ show only $\sim 12\%$ SDW volume fraction and such crystals also show long range magnetic correlations.⁶ Thus, if the system is microscopically phase separated into regions of typical size 15 Å - 50 Å, there must be coupling between SDW

regions via the intervening non-magnetic SC region. We suggest that the magnetic order parameter has a long tail inside the SC region with a magnetic moment that is below the μSR resolution.³³ This would give rise to percolation of the long-range order. We note that neutron scattering and μSR have different time scales, which must be taken into account in comparing the results.⁹ However, as demonstrated in Reference 9, despite their different energy resolutions μSR and neutron scattering measure exactly the same temperature dependence for the order parameter implying that they are seeing identical physics.

Our observation of competing SC and SDW order is unexpected in light of the coincident transition temperatures to SC and magnetic order. One possible explanation of this is that the transition occurs at a tetracritical point.^{29,32,34}

We conclude that there is an interesting interplay between the SDW and SC orders in the high T_c superconductors. Although the two kinds of order appear at the same temperature, there is clearly a competition between them. The muon experiments together with the sample variation we see suggest that microscopic electronic phase separation may occur when superconductivity sets in. The recent theory of Demler and Sachdev,²⁸ based on the assumption of the microscopic coexistence and competition between SC and SDW order parameters explains the field dependence of the SDW Bragg peak.

Acknowledgments

We have benefited from useful discussions with E. Demler, S. Sachdev, S.-C. Zhang, P. A. Lee and Y. J. Uemura. We thank T. Imai for discussions of the NMR and NQR results and for permission to summarize these results before publication. This work has been supported at MIT by the MRSEC Program of the National Science foundation under Award No. DMR 9808941, by NSF under Awards No. DMR 0071256 and DMR 99-71264. Work at the University of Toronto is part of the Canadian Institute for Advanced Research and is supported by the Natural Science and Engineering Research Council of Canada. We acknowledge the support of the National Institute of Standards and Technology, U.S. Department of Commerce, in providing the neutron facilities used in this work. Work at SPINS is based upon activities supported by the National Science Foundation under Agreement No. DMR-9986442.

* Presently at Department of Physics and Center for Material Science and Engineering, Massachusetts Institute of Technology, Cambridge, MA 02139.

¹ J. Rossat-Mignod, L. P. Regnault, C. Vettier, P. Bourges, P. Burlet, J. Bossy, J. Y. Henry and G. Lapertot, *Physica C* **185-189**, 86 (1991); H. A. Mook, M. Yethiraj, G. Aeppli,

- T. E. Mason, T. Armstrong, Phys. Rev. Lett. **70**, 3490 (1993); H. F. Fong, B. Keimer, P. W. Anderson, D. Reznik, F. Dogan, I. A. Aksay, Phys. Rev. Lett. **75**, 316 (1995).
- ² H. F. Fong, P. Bourges, Y. Sidis, L. P. Regnault, A. Ivanov, G. D. Gu, N. Koshizuka, B. Keimer, Nature **398**, 588 (1999).
 - ³ K. Yamada, C. H. Lee, K. Kurahashi, J. Wada, S. Wakimoto, S. Ueki, H. Kimura, Y. Endoh, S. Hosoya, G. Shirane, R. J. Birgeneau, M. Greven, M. A. Kastner, Y. J. Kim, Phys. Rev. B **57**, 6165 (1998).
 - ⁴ S. W. Cheong, G. Aeppli, T. E. Mason, H. Mook, S. M. Hayden, P. C. Canfield, Z. Fisk, K. N. Clausen, and J. L. Martinez, Phys. Rev. Lett. **67**, 1791 (1991).
 - ⁵ J. M. Tranquada, B. J. Sternlieb, J. D. Axe, Y. Nakamura, S. Uchida, Nature **375**, 561 (1995); N. Ichikawa, S. Uchida, J. M. Tranquada, T. Niemoller, P. M. Gehring, S.-H. Lee, and J. R. Schneider, Phys. Rev. Lett. **85**, 1738 (2000).
 - ⁶ H. Kimura, K. Hirota, H. Matsushita, K. Yamada, Y. Endoh, S.-H. Lee, C. F. Majkrzak, R. W. Erwin, G. Shirane, M. Greven, Y. S. Lee, M. A. Kastner, R. J. Birgeneau Phys. Rev. B **59**, 6517 (1999).
 - ⁷ Y. S. Lee, R. J. Birgeneau, M. A. Kastner, Y. Endoh, S. Wakimoto, K. Yamada, R. W. Erwin, S.-H. Lee, G. Shirane, Phys. Rev. B **60**, 3643 (1999).
 - ⁸ A. Savici, Y. Fudamoto, I. M. Gat, M. I. Larkin, Y. J. Uemura, K. M. Kojima, Y. S. Lee, M. A. Kastner, R. J. Birgeneau, Physica B **289-290**, 338 (2000).
 - ⁹ A. Savici, Y. Fudamoto, I. M. Gat, M. I. Larkin, Y. J. Uemura, G. M. Luke, K. M. Kojima, Y. S. Lee, M. A. Kastner, R. J. Birgeneau, K. Yamada, preprint cond-mat/0202037 (2002).
 - ¹⁰ J. Zaanen and O. Gunnarsson, Phys. Rev. B **40**, 7391 (1989).
 - ¹¹ V. J. Emery, S. A. Kivelson, and O. Zachar, Phys. Rev. B **56**, 6120 (1997).
 - ¹² S. R. White, D. J. Scalapino, Phys. Rev. Lett. **80**, 1272 (1998); *ibid.* **81**, 3227 (1998).
 - ¹³ R. S. Markiewicz, Phys. Rev. B **62**, 1252 (2000).
 - ¹⁴ I. Martin, G. Ortiz, A. V. Balatsky, A. Bishop, Int. J. Mod. Phys. B **14**, 3567 (2000); J.-X. Zhu, I. Martin, A. R. Bishop, cond-mat/0201519 (2002).
 - ¹⁵ Y. S. Lee, M. A. Kastner, R. J. Birgeneau, unpublished.
 - ¹⁶ F. C. Chou, J. H. Cho, and D. C. Johnston, Physica C **197**, 303 (1992); Z. G. Li, H. H. Feng, Z. Y. Yang, A. Hamed, S. T. Ting, P. H. Hor, S. Bhavaraju, J. F. DiCarlo, and A. J. Jacobson, Phys. Rev. Lett. **77**, 5413 (1996).
 - ¹⁷ P. Singer, A. Hunt and T. Imai, unpublished.
 - ¹⁸ B. O. Wells, Y. S. Lee, M. A. Kastner, R. J. Christianson, R. J. Birgeneau, K. Yamada, Y. Endoh, G. Shirane, Science **277**, 1067 (1997).
 - ¹⁹ B. O. Wells, R. J. Birgeneau, F. C. Chou, Y. Endoh, D. C. Johnston, M. A. Kastner, Y. S. Lee, G. Shirane, J. M. Tranquada, K. Yamada, Z. Phys. B **100**, 535 (1996).
 - ²⁰ S. Katano, M. Sato, K. Yamada, T. Suzuki, and T. Fukase, Phys. Rev. B **62**, R14677 (2000).
 - ²¹ B. Lake, G. Aeppli, K. N. Clausen, D. F. McMorro, K. Lefmann, N. E. Hussey, N. Mangkorntong, M. Nohara, H. Takagi, T. E. Mason, A. Schroder, Science **291**, 1759 (2001).
 - ²² B. Lake, H. M. Ronnow, N. B. Christensen, G. Aeppli, K. Lefmann, D. F. McMorro, P. Vorderwisch, P. Smeibidl, N. Mangkorntong, T. Sasegawa, M. Nohara, H. Takagi, T. E. Mason, Nature **415**, 299 (2001).
 - ²³ Y. J. Uemura, A. Keren, L. P. Le, G. M. Luke, W. D. Wu, Y. Kubo, T. Manako, Y. Shimakawa, M. Subramanian, J. L. Cobb and J. T. Markert, Nature **364**, 605 (1993).
 - ²⁴ Y. J. Uemura, Solid State Commun. **120**, 347 (2001), and references therein.
 - ²⁵ D. C. Johnston, Phys. Rev. Lett. **62**, 957 (1989).
 - ²⁶ T. Nakano, M. Oda, C. Manabe, N. Momono, Y. Miura, and M. Ido, Phys. Rev. B **49**, 16000 (1994).
 - ²⁷ A. Weinrib and B. I. Halperin, Phys. Rev. B **27**, 413 (1983).
 - ²⁸ E. Demler, S. Sachdev, and Y. Zhang, Phys. Rev. Lett. **87**, 067202 (2001).
 - ²⁹ S.-C. Zhang, Science **275**, 1089 (1997); J.-P. Hu and S.-C. Zhang, preprint cond-mat/0108273 (2001).
 - ³⁰ For a recent review, E. H. Brandt, Rep. Prog. Phys., **58**, 1465 (1995).
 - ³¹ Y. Ando, G. S. Boebinger, A. Passner, L. F. Schneemeyer, T. Kimura, M. Okuya, S. Watauchi, J. Shimoyama, K. Kishio, K. Tamasaku, N. Ichikawa, and S. Uchida, Phys. Rev. B **60**, 12475 (1999).
 - ³² S. Kivelson, G. Aeppli, V. J. Emery, PNAS **98**, 11903 (2001).
 - ³³ P. A. Lee, private communication.
 - ³⁴ A. Aharony, preprint cond-mat/0107585 (2001); preprint cond-mat/0201576 (2002).